Article

Theoretical Analysis on Absorption of Carbon Dioxide (CO$_2$) into Solutions of Phenyl Glycidyl Ether (PGE) Using Nonlinear Autoregressive Exogenous Neural Networks

Naveed Ahmad Khan [1] , Muhammad Sulaiman [1,*] , Carlos Andrés Tavera Romero [2] and Fawaz Khaled Alarfaj [3]

[1] Department of Mathematics, Abdul Wali Khan University Mardan, Mardan 23200, Khyber Pakhtunkhwa, Pakistan; ahmednaveed854477@gmail.com

[2] COMBA R&D Laboratory, Faculty of Engineering, Universidad Santiago de Cali, Cali 76001, Colombia; carlos.tavera00@usc.edu.co

[3] Department of Computer and Information Sciences, Imam Mohammad Ibn Saud Islamic University, Alhasa 31982, Saudi Arabia; fkarfaj@imamu.edu.sa

* Correspondence: msulaiman@awkum.edu.pk

Abstract: In this paper, we analyzed the mass transfer model with chemical reactions during the absorption of carbon dioxide (CO$_2$) into phenyl glycidyl ether (PGE) solution. The mathematical model of the phenomenon is governed by a coupled nonlinear differential equation that corresponds to the reaction kinetics and diffusion. The system of differential equations is subjected to Dirichlet boundary conditions and a mixed set of Neumann and Dirichlet boundary conditions. Further, to calculate the concentration of CO$_2$, PGE, and the flux in terms of reaction rate constants, we adopt the supervised learning strategy of a nonlinear autoregressive exogenous (NARX) neural network model with two activation functions (Log-sigmoid and Hyperbolic tangent). The reference data set for the possible outcomes of different scenarios based on variations in normalized parameters $(\alpha_1, \alpha_2, \beta_1, \beta_2, k)$ are obtained using the MATLAB solver "pdex4". The dataset is further interpreted by the Levenberg–Marquardt (LM) backpropagation algorithm for validation, testing, and training. The results obtained by the NARX-LM algorithm are compared with the Adomian decomposition method and residual method. The rapid convergence of solutions, smooth implementation, computational complexity, absolute errors, and statistics of the mean square error further validate the design scheme's worth and efficiency.

Keywords: carbon dioxide; phenyl glycidyl ether; reaction mechanisms; reaction kinetics and diffusion; chemical reactivity concentration of CO$_2$ and PGE; artificial intelligence; machine learning; NARX networks

1. Introduction

Carbon dioxide is a generally useful gas made up of a carbon and two oxygen atoms. It is essential in plant photosynthesis, manufacturing carbonated soft drinks, powering pneumatic systems in robots, fire extinguishers, removing caffeine from coffee [1,2], etc. Carbon dioxide has the potential to be a significant and inexpensive carbon source. Its environmental impact as a greenhouse gas could be reduced by converting it into valuable products. The chemical conversion and fixation of carbon dioxide into valuable substances with desirable solutions has become an essential topic of research because of the danger posed by global warming. The conversion of carbon dioxide into useful chemicals is a very appealing approach [3].

Well-known examples include the oxirane reaction leading to a five-member cyclic carbonate [3], porous polymer bead-supported ionic liquids for the synthesis of cyclic carbonate [4,5], zeolite-based organic–inorganic hybrid catalysts for phosgene-free and

solvent-free synthesis of cyclic carbonates, and carbamates [6,7]. Such carbonates are used as polymer synthesis sources and patented polar solvents.

The reaction kinetics of CO_2 and phenyl glycidyl ether (PGE) was investigated by Park, and Choe [8] in a heterogeneous system during the chemical absorption of carbon dioxide into PGE solutions containing the catalyst THA–CP–MS41. The phenomena of absorption is modeled by nonlinear differential equations, which were solved by Wazwaz and Singh [9] to relate the steady-state concentration of CO_2 and PGE using the homotopy analysis method.

S. Muthukaruppan [10] applied the Adomian decomposition method for the heat transfer of chemical reaction between CO_2 and PGE solutions. Various numerical and analytical techniques, such as Laplace homotopy analysis method (LHAM) [11], homotopy perturbation transform method (HPTM) [12], optimal homotopy analysis method (OHAM) [13], conformable Adomian decomposition method (CADM) [14], and Haar wavelet method (HWM) [15], were developed to solve nonlinear differential equations governing reaction-diffusion equations of chemical kinetics.

In recent times, stochastic computing paradigms based on artificial intelligence have been used extensively to find numerical solutions for different problems arising in various fields, such as fuzzy systems [16–18], petroleum engineering [19], carbon capture process [20–22], wire coating dynamics [23], biological systems [24,25], civil engineering [26,27], coal-fired power plant retrofitted [28], and electrical and thermal engineering [29–31]. These contributions motivated the authors to investigate the absorption of carbon dioxide (CO_2) into solutions of phenyl glycidyl ether (PGE) by strengthening the computational ability of neural networks. Salient features of the presented study are summarized as:

- A mathematical model for chemical analysis and absorption of carbon dioxide (CO_2) into phenyl glycidyl ether (PGE) solutions is presented. Furthermore, a novel stochastic technique based on nonlinear autoregressive exogenous (NARX) neural networks with the Levenberg–Marquardt algorithm is utilized to optimize the system of singular nonlinear differential equations for the normalized concentration of CO_2 and PGE.
- The design scheme NARX-LM algorithm with two different activations function (Log-sigmoid and Hyperbolic tangent) is implemented to investigate the influence of variations in normalized parameters such α_1, α_2, β_1 and β_2 on concentration profiles of CO_2 and PGE.
- To validate the accuracy of the design supervised learning mechanism, the results obtained are compared with the residual method, the Adomian decomposition method, machine learning algorithms, and numerical solution.
- Extensive graphical analysis based on absolute errors, fitting of numerical and approximate solutions, absolute errors, and performance graphs of mean square error are plotted to further validate the worth of the design scheme.

2. Problem Formulation

Figure 1 demonstrates the experimental setup for stirred-cell absorber, where A, B, C are valves, D is the absorber, E is the impeller, F shows the bottle of liquid, G represents the funnel, H is the soap film meter, and I is the gas chromatographer [8]. The chemical reaction between carbon dioxide and phenyl glycidyl ether for the formation of a five membered cyclic carbonate is shown in Figure 2. Here, R is a functional group $(-CH_2 - O - C_6H_5)$. An overall reaction in Figure 2 consists of two steps, a reversible reaction between PGE(B) and THA-CP-MS41 (QX) is used to form an intermediate complex C_1 in the first step. In the second step, QX and five membered cyclic carbonate (C) is formed by a reversible reaction between CO_2 and C_1.
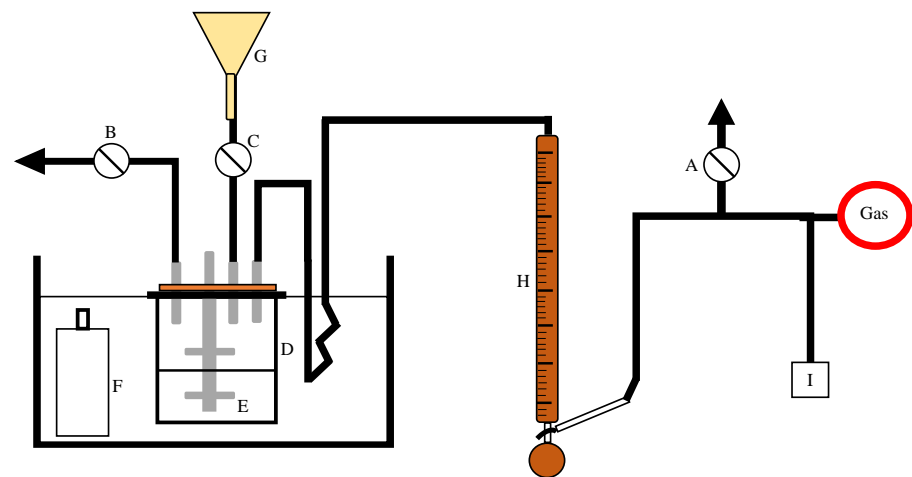
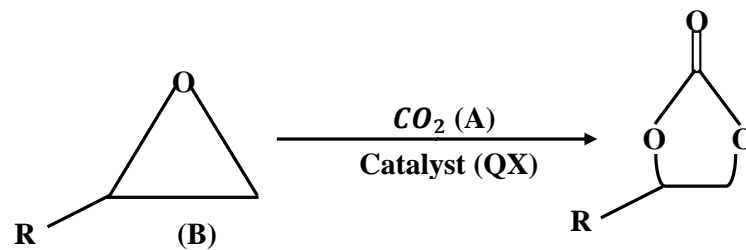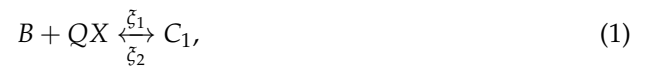**Figure 1.** The schematic view of the stirred cell absorber.

Figure 2. The overall reaction between CO_2 and PGE.

$$B + QX \xrightleftharpoons[\xi_2]{\xi_1} C_1, \tag{1}$$

$$A + C_1 \longrightarrow \xi_3 C + QX, \tag{2}$$

In a steady state, the chemical reaction rate of CO_2 to C_1 is given as

$$r_{A,cons} = \frac{S_t C_B}{\frac{1}{\Theta_1 \xi_3 C_A} + \frac{1}{\xi_1} + \frac{C_B}{\xi_3 C_A}}, \tag{3}$$

where C_A and C_B denotes the concentration of CO_2 and PGE, S_t is the surface area of the catalyst, and Θ_1 denotes the reaction equilibrium. ξ_1 and ξ_2 denote the forward reaction constants in Equations (2) and (3), respectively. The nonlinear mass balances of CO_2 and PGE as a result of the subsequent chemical reactions are shown in Equations (4) and (5) as

$$D_A \frac{d^2 C_A(z)}{dz^2} = \frac{S_t C_B(z)}{\frac{1}{\Theta_1 \xi_3 C_A(z)} + \frac{1}{\xi_1} + \frac{C_B(z)}{\xi_3 C_A(z)}}, \tag{4}$$

$$D_B \frac{d^2 C_B(z)}{dz^2} = \frac{S_t C_B(z)}{\frac{1}{\Theta_1 \xi_3 C_A(z)} + \frac{1}{\xi_1} + \frac{C_B(z)}{\xi_3 C_A(z)}}, \tag{5}$$

where D_A and D_B are parameters for the measure of diffusion of CO_2 and PGE, respectively, z is distance. Boundary conditions for problem are

$$\text{at} \quad z = 0; \quad C_A = C_{Ai}, \quad \frac{dC_B}{dz} = 0, \tag{6}$$

$$\text{at} \quad z = z_L; \quad C_A = C_{AL}, \quad C_B = C_{Bo}, \tag{7}$$

The following dimensionless parameters are defined to normalize Equations (4) and (5) along with the boundary conditions.

$$u = \frac{C_A}{C_{Ai}}, \quad v = \frac{C_B}{C_{Bo}}; \quad x = \frac{z}{z_L}, \quad \alpha_1 = \frac{z_L^2 s_t C_{Bo} \Theta_1 \xi_3}{D_A}$$
$$\alpha_2 = \frac{z_L^2 s_t C_{Ai} \Theta_1 \xi_3}{D_B}, \quad \beta_1 = \frac{C_{Ai} \Theta_1 \xi_3}{\xi_1}, \quad \beta_2 = \frac{C_{Bo} \Theta_1 \xi_1}{\xi_1}, \tag{8}$$

Now, using Equation (8), the nonlinear equations for diffusion of CO_2 and PGE can be written as

$$\frac{d^2 u(x)}{dx^2} - \frac{\alpha_1 u(x) v(x)}{1 + \beta_1 u(x) + \beta_2 v(x)} = 0, \tag{9}$$

$$\frac{d^2(v)}{dx^2} - \frac{\alpha_2 u(x) v(x)}{1 + \beta_1 u(x) + \beta_2 v(x)} = 0, \tag{10}$$

The dimensionless boundary conditions are given as

$$\text{At} \quad x = 0 \quad u = 1, \quad \frac{dv}{dx} = 0, \tag{11}$$

$$\text{At} \quad x = 1 \quad u = k, \quad v = 1. \tag{12}$$

Here, the normalized concentrations of CO_2 and PGE are denoted by $u(x)$ and $v(x)$, respectively. α_1, α_2, β_1, and β_2 are normalized parameters. The distance from the center is x, and $k = \frac{C_{AL}}{C_{Ai}}$ is the concentration of CO_2 at the catalyst surface, and its value is less than 1. The enhancement factor of carbon dioxide and ratio of the flux (β) of the chemical reaction is defined as

$$\beta = -\left(\frac{du}{dx}\right)_{x=0}. \tag{13}$$

3. Design Methodology

3.1. Artificial Neural Networks and NARX Model

Artificial Neural Networks (ANN's) are used for an extensive range of problems in clustering, pattern classification, function approximation, recognition, optimization, and prediction [32,33]. ANNs are mathematical tools that are stimulated by the biological brain system, and they have a tremendous ability to learn, store, and remember data. They are black-box modelling tool that can perform non-linear mapping from an n-dimensional input space to an m-dimensional output space while the input and output spaces are unknown [34].

The choice of ANN model depends on the prior knowledge of the system to be modeled. The basic idea of NARX is a nonlinear version of the Autoregressive Exogenous (ARX) instrument, which is a common tool for identifying linear black-box systems. The NARX models are extensively used for modeling number of nonlinear dynamical system, such as dual response regulators interact with dual sensors [35], chaotic time series prediction [36], prediction of the daily direct solar radiation [37], and long-term time series prediction [38]. A recurrent dynamic neural network, or NARX, is a type of neural network that learns from previous experiences. It features feedback links that encircle the network in multiple levels.

NARX has two different architectures named series-parallel architecture (open-loop) and parallel architecture (close-loop) as shown in Figure 3. In this study, a parallel architecture NARX model is adopted to study the concentration and absorption of CO_2 into a PGE solution. The general NARX model is given as

$$\hat{y}(t+1) = F\left(\begin{array}{c} y(t), y(t-1), \ldots, y(t-n_y), x(t+1) \\ x(t), x(t-1), \ldots, x(t-n_x) \end{array} \right) \tag{14}$$
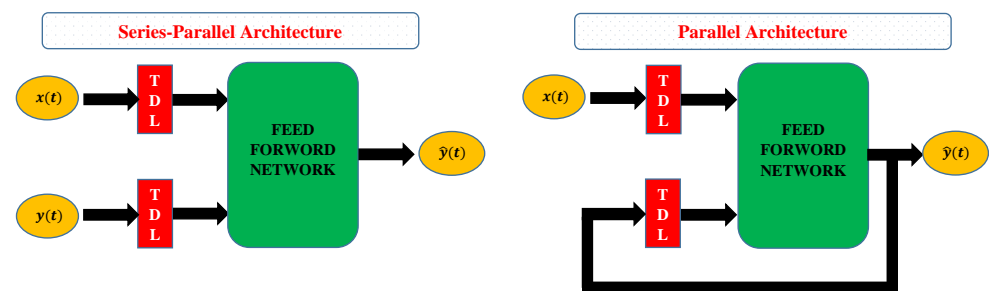
Figure 3. Architectures of the NARX neural network.

Here, t represents the time period, $\hat{y}(t+1)$ is output of the NARX at time t, and n_x and n_y are the input and output delays. $F(.)$ is the mapping function of the neural networks. The basic advantage of using parallel architecture is that the usual training algorithm for Multi-Layer Perceptron (MLP) can be used for training neurons. The MLP offers a powerful structure that allows learning any type of continuous nonlinear mapping. A traditional MLP has three layers: input, hidden, and output. Neurons, activation functions, and weights are the other components.

In this study, we used two activation functions named the Log-sigmoid and Hyperbolic tangent. The convergence speed of these functions is much higher then other activation functions. The optimal gradient factors for Logsigmoid and Hyperbolic tangent are greater than those for Normal, Cauchy, Erf-Logsig and Laplace activations functions, which make them unique. The mathematical form for these activation functions are given by Equations (15) and (16), respectively.

$$f_1(x) = \frac{1}{1 + e^{-x}}, \tag{15}$$

$$f_2(x) = \frac{e^x - e^{-x}}{e^x + e^{-x}}, \tag{16}$$

The detailed structure of neurons along with different layers of MLP network are shown in Figure 4. The motivation of using NARX model with respect to other neural networks model is its speed of convergence and needs of less training cycles [39]. It provides the description of the system in terms of nonlinear function of delayed inputs, outputs, and their predicted errors. Thus, NARX model generalizes any nonlinear dynamical system and can be applied to various problems of different fields, such as nonlinear filtering, prediction, chaotic time series prediction, control, and time series modeling [40].
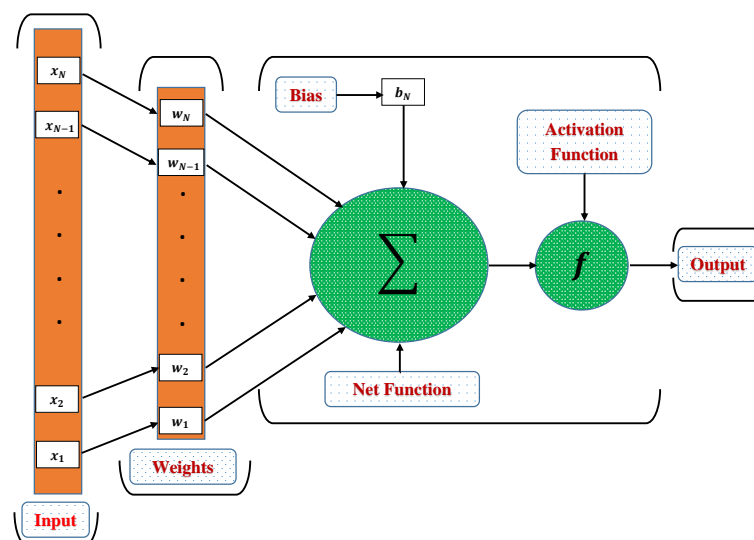

Figure 4. Details of a neuron in an MLP network.

3.2. Learning Procedure and Performance Indicators

In this section, the working and training procedure of neurons is discussed. An appropriate algorithm is used to train the weights for calculating an approximate solution for the problem. During the training phase, a network is presented with a set of inputs and their desired output (also known as target data). A reference solution or target data of 1001 points is generated by using the numerical solver "Pdex4" in MATLAB. Furthermore, the data and weights are tuned by backpropogated Levenberg–Marquardt algorithm using "nntool" for proper training, validation, and testing. The sample of 1001 points is divided as

- 75% (701 samples) are used for training.
- 15% (150 samples) are used for validation.
- 15% (150 samples) are used for testing.

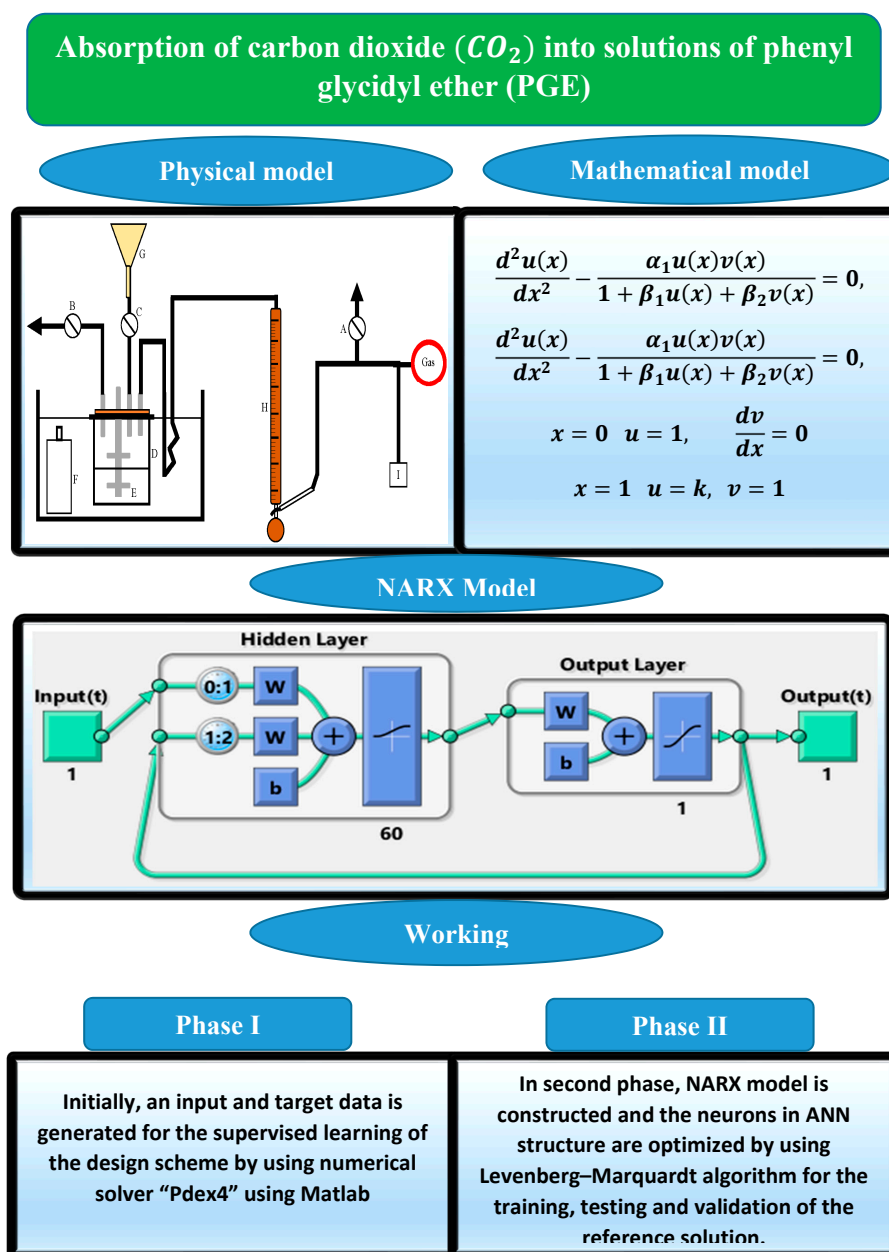Figure 5 shows the model of the problem, NARX model, and workflow of the design scheme.

Figure 5. Mathematical model of the problem, NARX model, and workflow of the design scheme.

The performance of design scheme are measures of the performance indicators in terms of the mean square error (MSE) of the fitness function of the model, regression R^2, error histograms, and absolute errors (AE). The mathematical formulation of the MSE, R^2, and AE are given as

$$\text{MSE} = \frac{1}{m} \sum_{j=1}^{m} \left(x_j(t) - \hat{x}_j(t) \right)^2, \tag{17}$$

$$R^2 = 1 - \frac{\sum_{j=1}^{m} \left(\hat{x}_j(t) - \bar{x}_j(t) \right)^2}{\sum_{j=1}^{m} \left(x_j(t) - \bar{x}_j(t) \right)^2}, \tag{18}$$

and

$$\text{AE} = \left| x_j(t) - \hat{x}_j(t) \right|, \quad j = 1, 2, \ldots, m. \tag{19}$$

where, x_j, $\bar{x}_j$, and $\hat{x}_j$ denote the reference, approximate, and mean of the solution at the *jth* input, and m is the number of mesh points. The desire value of MSE and AE for perfect fitting is equal to zero, while the value of R^2 is one.

4. Reference Solutions

In the literature, various methods have been developed to study the concentration of carbon dioxide, phenyl glycidyl ether, and enhancement factors.

Approximate solutions obtained by the the Adomian decomposition method and Duan–Rach modified (ADM and DRM) [41] are

$$u(x) = 1 - \left[\frac{x(1-x)\alpha_1 + 2(1-k)(1+\beta_1+\beta_2)}{2(1+\beta_1+\beta_2)} \right] + \frac{xa_1}{24(1+\beta_1+\beta_2)^3}$$
$$\left[5\alpha_2(1+\beta_1) + a_1(1+\beta_2) + 4(1-k)(1+\beta_2)(1+\beta_1+\beta_2) - x \left(\begin{array}{c} (6-x^2)\alpha_2(1+\beta_1) + (2-x)xa_1(1+\beta_2) \\ +4(1-k)x(1+\beta_2)(1+\beta_1+\beta_2) \end{array} \right) \right] \tag{20}$$

$$v(x) = 1 - \frac{(1-x^2)\alpha_2}{2(1+\beta_1+\beta_2)} + \frac{\alpha_2}{24(1+\beta_1+\beta_2)^3}$$
$$\left[5\alpha_2(1+\beta_1) + \alpha_1(1+\beta_2) + 4(1-k)(1+\beta_2)(1+\beta_1+\beta_2) - x^2 \left(\begin{array}{c} (6-x^2)\alpha_2(1+\beta_1) + (2-x)x\alpha_1(1+\beta_2) \\ +4(1-k)x(1+\beta_2)(1+\beta_1+\beta_2) \end{array} \right) \right] \tag{21}$$

Approximate solutions obtained by the domian decomposition method [10] are

$$u(x) = (k-1)x + 1 + \frac{\alpha_1 x}{2\beta_1}(x-1) - \frac{\alpha_1(1+\beta_2)}{\beta_1^3(k-1)^2} [\log(1+\beta_2+\beta_1) - 1](1+\beta_2+\beta_1)(x-1)$$
$$\frac{\alpha_1(1+\beta_2)}{\beta_1^3(k-1)^2} \left[\begin{array}{c} (\log(1+\beta_2+\beta_1((k-1)x+1)-1))(\log(1+\beta_2+\beta_1((k-1)x+1)-1)) \\ -x(\log(1+\beta_2+\beta_1 k) - 1)(1+\beta_2+\beta_1 k) \end{array} \right], \tag{22}$$

$$v(x) = 1 + \frac{\alpha_2}{2\beta_1}\left(x^2 - 1 \right) + \frac{\alpha_2(1+\beta_2)(x-1)}{\beta_1^2(k-1)} [\log(1+\beta_2+\beta_1)]$$
$$- \frac{\alpha_2(1+\beta_2)}{\beta_1^3(k-1)^2} \left[\begin{array}{c} (\log(1+\beta_2+\beta_1((k-1)x+1)-1))(1+\beta_2+\beta_1((k-1)x+1)-1)) \\ -(\log(1+\beta_2+\beta_1 k) - 1)(1+\beta_2+\beta_1 k) \end{array} \right] \tag{23}$$

Approximate solutions obtained by the Adomian Daftarder–Jafari method [42] are

$$u(x) = x + \frac{x^4\alpha_1}{12} + \frac{x^7\alpha_1^2}{504} + \frac{x^7\alpha_1\alpha_2}{504} + \frac{x^{10}\alpha_1^2\alpha_2}{12960} - \frac{x^5 a_1\beta_1}{20} - \frac{x^8\alpha_1^2\beta_1}{672} - \frac{x^5 a_1\beta_2}{20} - \frac{x^8\alpha_1\alpha_2\beta_2}{672}, \tag{24}$$

$$v(x) = x + \frac{x^4\alpha_2}{12} + \frac{x^7\alpha_1\alpha_2}{504} + \frac{x^7\alpha_2^2}{504} + \frac{x^{10}\alpha_2^2\alpha_1}{12960} - \frac{x^5 a_2\beta_1}{20} - \frac{x^8 a_1 a_2\beta_1}{672} - \frac{x^5 a_2\beta_2}{20} - \frac{x^8\alpha_2^2\beta_2}{672}, \tag{25}$$

The approximate solutions obtained by the Residual method [43] are

$$u(x) = k \frac{\sinh\left(\sqrt{\frac{\alpha_1}{1+\beta_1 k+\beta_2}}x\right)}{\sinh\left(\sqrt{\frac{\alpha_1}{1+\beta_1 k+\beta_2}}\right)} + \frac{\sinh\left(\sqrt{\frac{\alpha_1}{1+\beta_1 k+\beta_2}}(1-x)\right)}{\sinh\left(\sqrt{\frac{\alpha_1}{1+\beta_1 k+\beta_2}}\right)} \tag{26}$$

$$v(x) = \frac{\cosh\left(\sqrt{\frac{\alpha_2 k}{1+\beta_1 k+\beta_2}}x\right)}{\cosh\left(\sqrt{\frac{\alpha_2 k}{1+\beta_1 k+\beta_2}}\right)}, \tag{27}$$

5. Numerical Experimentation and Discussion

In this section, the design scheme NARX-LM algorithm is applied to study the concentration of CO_2 and PGE solution under influence of variations in normalized parameters. Figure 6a,b represents the effect of variations in k on CO_2 and PGE with $\alpha_1 = \alpha_2 = \beta_1 = 1$ and $\beta_2 = 3$. Figure 6c illustrates the influence of variations in α_2 with $\alpha_1, \beta_1 = 100, k = 0.1$ and $\beta_2 = 10$. Variations in β_1 and β_2 with fixed values of $\alpha_1 = \alpha_2 = 1$ and $k = 0.1$ are shown through Figure 6d,e, respectively. It can be seen that concentration of CO_2 increases with increase in k.

The diffusivity of PGE decreases with increases in the surface catalyst. Influence of variations in flux (Enhancement factor) was investigated and the results are demonstrated in Figure 7. The value of flux decreases with increase in β_1 and β_2 while it increase with increase in α_1. Further, to study, the results of design scheme different cases of Equations (9) and (10) are considered. Csse I: $k = 0.1, \beta_1 = 0.1, \beta_2 = 0.001, \alpha_1 = 1$ and $\alpha_2 = 1$, Case II: $k = 0.5, \beta_1 = 1, \beta_2 = 3, \alpha_1 = 2$ and $\alpha_2 = 2$, Case III: $k = 0.1, \beta_1 = 100, \beta_2 = 10, \alpha_1 = 1$ and $\alpha_2 = 50$ and Case IV: $k = 0.5, \beta_1 = 1, \beta_2 = 3, \alpha_1 = 2$, and $\alpha_2 = 5$.
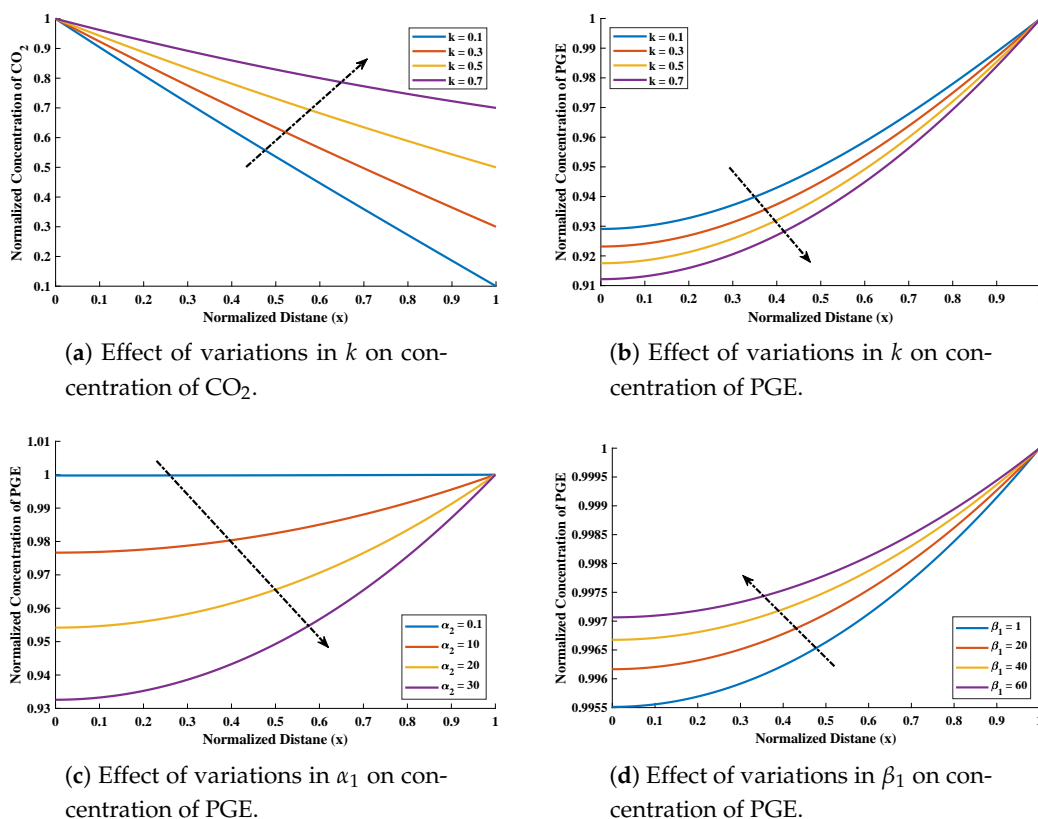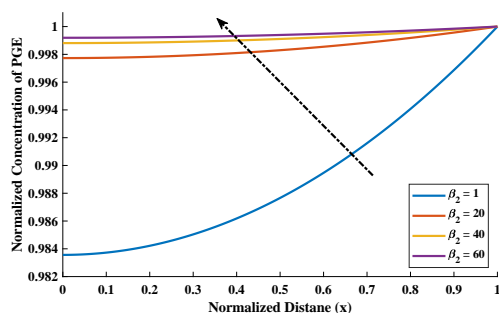

(**a**) Effect of variations in k on concentration of CO_2.

(**b**) Effect of variations in k on concentration of PGE.

(**c**) Effect of variations in α_1 on concentration of PGE.

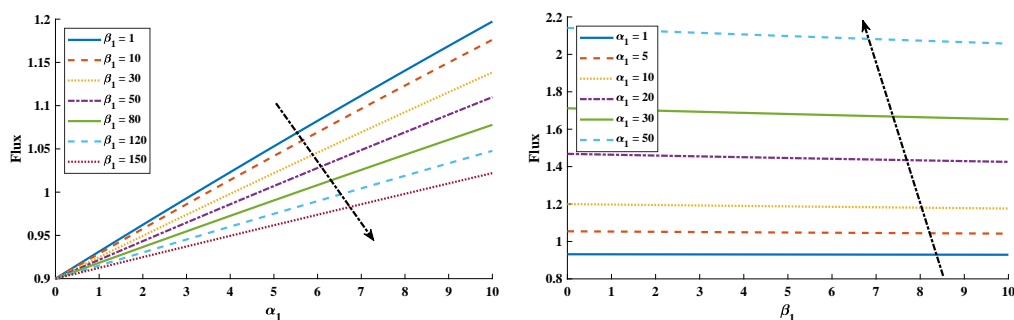(**d**) Effect of variations in β_1 on concentration of PGE.
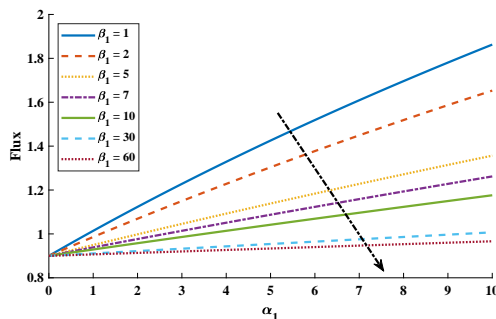
Figure 6. *Cont.*

(**e**) Effect of variations in β_2 on concentration of PGE.

Figure 6. Influence of variations in different parameters on the normalized concentration of CO_2 and PGE.

(**a**) Effect of variations in β_1.

(**b**) Effect of variations in α_1.

(**c**) Effect of variations in β_1

Figure 7. Influence of variations on the normalized parameter flux (enhancement factor).

The statistics of approximate solutions obtained by NARX-NM algorithm for steady state concentration profiles of CO_2 and PGE are compared with the Adomian decomposition method and Duan–Rach modified (ADM and DRM) [41], Adomian decomposition method (ADM) [10], Residual method [43], and numerical method as shown in Tables 1 and 2. The results in terms of absolute errors obtained by NARX-LM algorithm are compared with machine learning techniques, such as feed-forward backpropogated (FF) and Layer-Recurrent (LR) neural networks. Tables 3 and 4 shows that solutions obtained by proposed technique are in good agreement with analytical solutions as compared to other neural networks.

The fitting of approximate solutions by the design algorithm with reference data for different cases of Equations (9) and (10) are shown in Figure 8. The absolute errors (AE) in our solutions are shown through Figures 8 and 9. It can be seen that solutions by NARX-LM algorithm overlaps the numerical solutions with AE that lies around 10^{-6} to 10^{-8}, 10^{-7} to 10^{-9}, 10^{-6} to 10^{-8} and 10^{-7} to 10^{-8}, respectively. The performance of the design scheme for two activation functions in term of mean square error are shown in Figure 10.
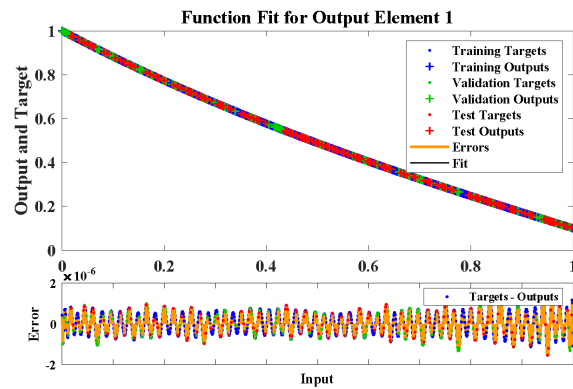
(**a**) $k = 0.1, \beta_1 = 0.1, \beta_2 = 0.001, \alpha_1 = 1$ and $\alpha_2 = 1$
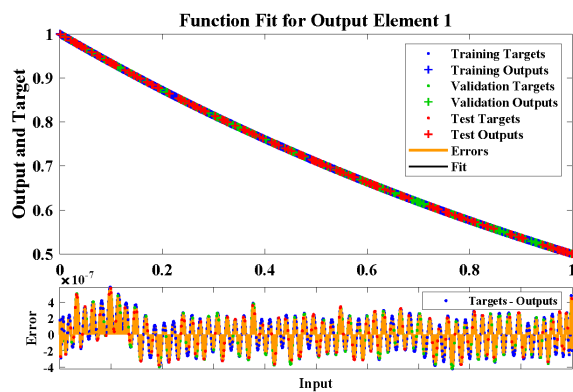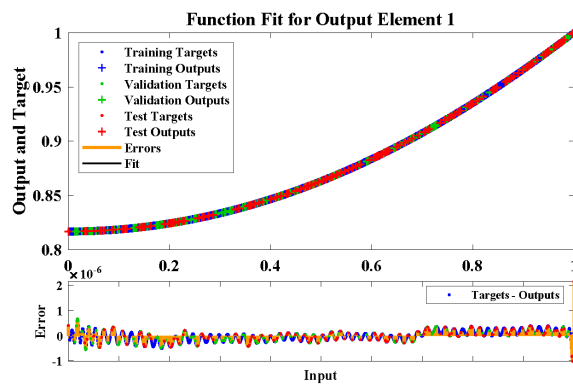
(**b**) $k = 0.5, \beta_1 = 1, \beta_2 = 3, \alpha_1 = 2$ and $\alpha_2 = 2$

(**c**) $k = 0.1, \beta_1 = 100, \beta_2 = 10, \alpha_1 = 1$ and $\alpha_2 = 50$

(**d**) $k = 0.5, \beta_1 = 1, \beta_2 = 3, \alpha_1 = 2$ and $\alpha_2 = 2$

Figure 8. (**a**,**b**) The fitting of numerical solution with the results obtained by the NARX-LM algorithm for the concentration of CO_2 and (**c**,**d**) the concentration of PGE.
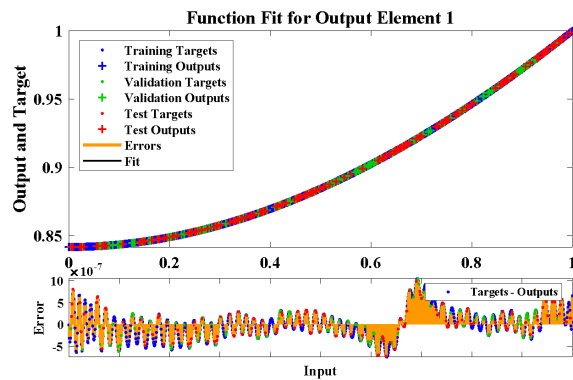
(**a**) $k = 0.1, \beta_1 = 0.1, \beta_2 = 0.001, \alpha_1 = 1$ and $\alpha_2 = 1$

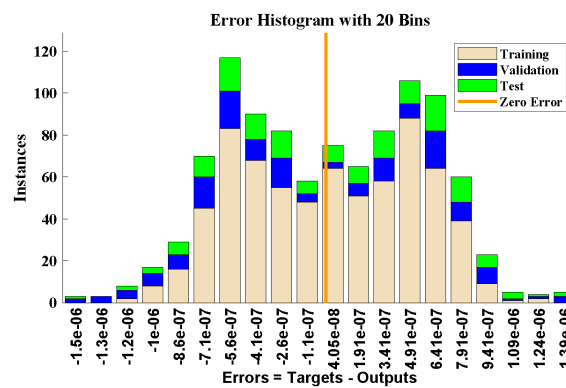(**b**) $k = 0.5, \beta_1 = 1, \beta_2 = 3, \alpha_1 = 2$ and $\alpha_2 = 2$

(**c**) $k = 0.1, \beta_1 = 100, \beta_2 = 10, \alpha_1 = 1$ and $\alpha_2 = 50$
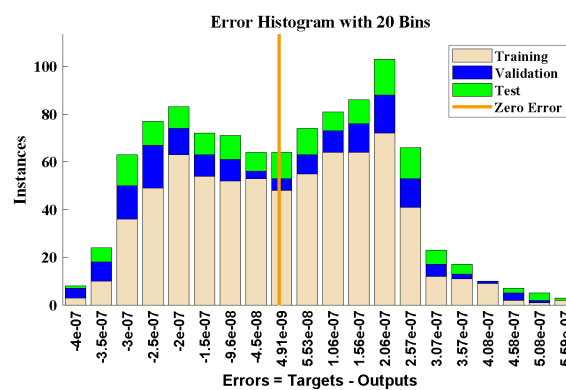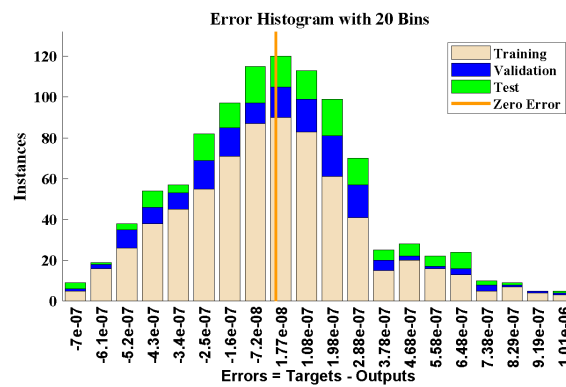

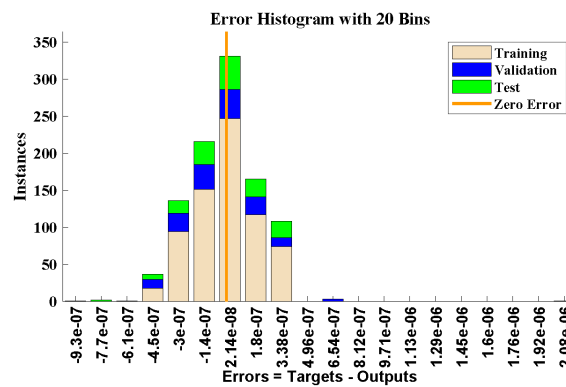(**d**) $k = 0.5, \beta_1 = 1, \beta_2 = 3, \alpha_1 = 2$ and $\alpha_2 = 2$

Figure 9. (**a**,**b**) The error histogram analysis for the concentration of CO_2 and (**c**,**d**) the errors in solution for the concentration of PGE.

(**a**) Case I

(**b**) Case II

(**c**) Case III

(**d**) Case IV

(**e**) Case I

(**f**) Case II

(**g**) Case III

(**h**) Case IV

Figure 10. (**a–d**) The convergence value of the performance function using the hyperbolic tangent sigmoid function and (**e–h**) the results of the performance function with the Log-sigmoid activation function.

The values of the mean square error obtained with the hyperbolic tangent sigmoid function for different cases are 1.4774×10^{-08}, 2.1953×10^{-08}, 4.1685×10^{-09} and 1.3712×10^{-08} with gradient 5.7587×10^{-08}, 9.2706×10^{-08}, 9.1040×10^{-08} and 8.1414×10^{-08}, respectively. The statistics of the performance function with the Log-sigmoid activation function for different cases are 1.0854×10^{-09}, 1.2073×10^{-08}, 1.0856×10^{-09} and 5.8732×10^{-09} with gradient 5.6208×10^{-07}, 2.2750×10^{-09}, 9.7326×10^{-08}, and 9.9145×10^{-08}, respectively.

Table 1. Comparison of the solutions obtained by the NARX-LM algorithm with the numerical results, NM, ADM, and DRM for the steady state concentration of CO_2.

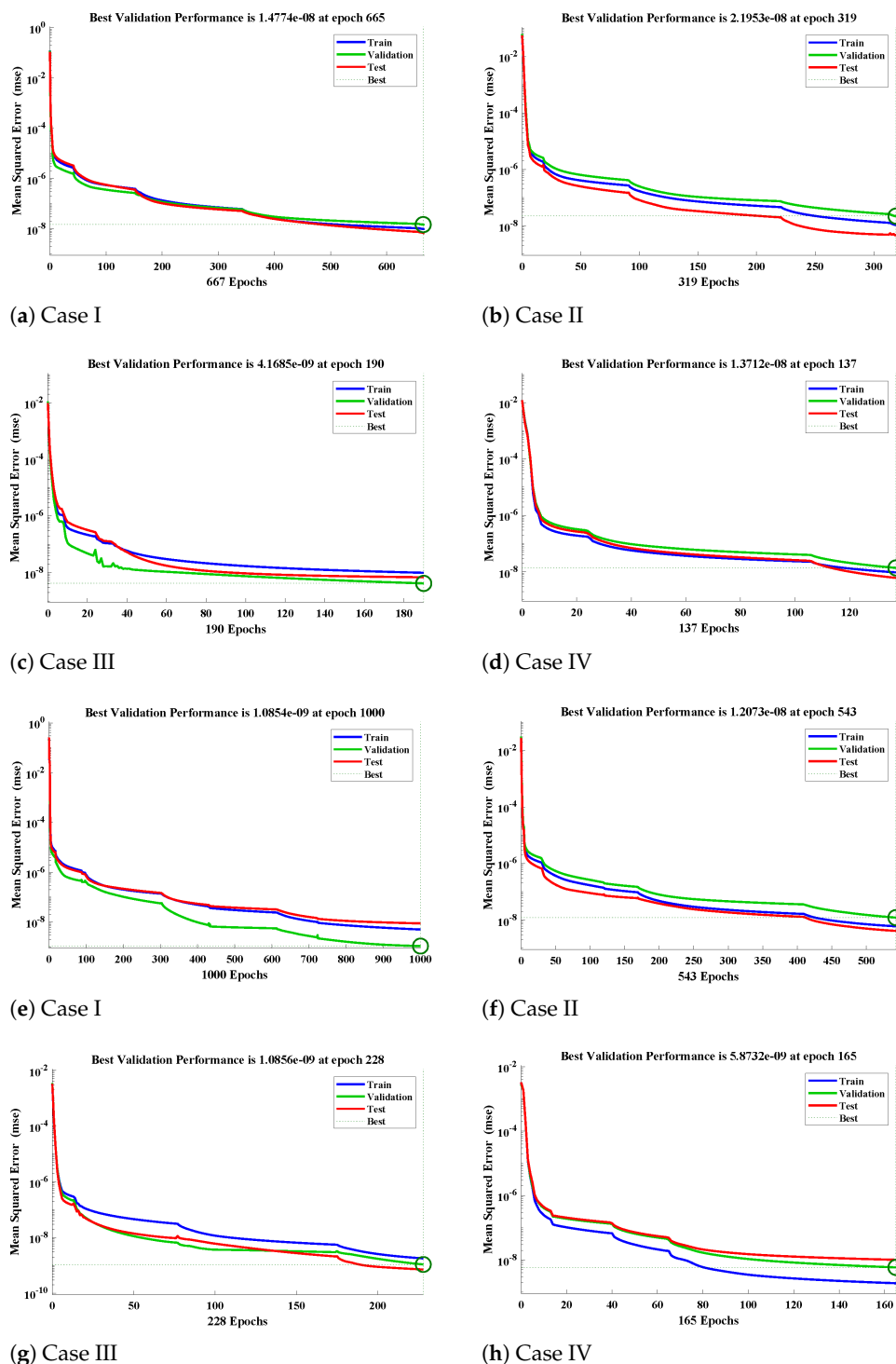|	$k = 0.1, \beta_1 = 0.1, \beta_2 = 0.001, \alpha_1 = 1$ and $\alpha_2 = 1$					$k = 0.5, \beta_1 = 1, \beta_2 = 3, \alpha_1 = 2$ and $\alpha_2 = 2$				
x	ADM & DRM	ADM	RM	Numerical	NARX-LM	ADM & DRM	ADM	RM	Numerical	NARX-LM
0	1	1	1	1	**1**	1	1	1	1	**1**
0.2	0.7721	0.7722	0.7733	0.7754	**0.7754**	8734	8734	8730	8740	**8740**
0.4	0.5746	0.5746	0.5773	0.5797	**0.5797**	7614	7614	7610	7620	**7620**
0.6	0.401	0.4011	0.4042	0.4061	**0.4061**	6629	6629	6626	6629	**6629**
0.8	0.2451	0.2451	0.2472	0.2482	**0.2482**	5762	5762	5761	5758	**5758**
1.0	0.1	0.1	0.1	0.1	**0.1**	0.5	0.5	0.5	0.5	**0.5**

Table 2. Comparison of the solutions obtained by the NARX-LM algorithm with the numerical results, NM, ADM, and DRM for the steady state concentration of PGE.

	$k = 0.1, \beta_1 = 100, \beta_2 = 10, \alpha_1 = 1$ and $\alpha_2 = 50$					$k = 0.5, \beta_1 = 1, \beta_2 = 3, \alpha_1 = 2$ and $\alpha_2 = 2$				
x	ADM & DRM	ADM	RM	Numerical	NARX-LM	ADM & DRM	ADM	RM	Numerical	NARX-LM
0	0.8199	0.8098	0.8199	0.8173	**0.8173**	0.8426	0.842	0.8426	0.842	**0.842**
0.2	0.827	0.8188	0.827	0.826	**0.826**	0.8497	0.8491	0.8497	0.8489	**0.8489**
0.4	0.8483	0.8459	0.8483	0.8478	**0.8478**	0.8701	0.8698	0.8701	0.8688	**0.8688**
0.6	0.8839	0.881	0.8839	0.8849	**0.8849**	0.9026	0.9021	0.9026	0.9023	**0.9023**
0.8	0.9342	0.9331	0.9342	0.9345	**0.9345**	0.9462	0.9459	0.9462	0.9471	**0.9471**
1.0	1	1	1	1	**1**	1	1	1	1	**1**

Table 3. Comparison of the absolute errors in solutions for the concentration of CO_2 obtained by the NARX-LM algorithm with different machine learning techniques for Case I and II.

	Case I			Case II		
x	FF-NN	LR-NN	NARX-LM	FF-NN	LR-NN	NARX-LM
0.0	7.567414×10^{-04}	1.976408×10^{-03}	$\mathbf{3.664701 \times 10^{-04}}$	1.853876×10^{-03}	1.611739×10^{-03}	$\mathbf{1.594322 \times 10^{-04}}$
0.1	2.294808×10^{-05}	3.465679×10^{-05}	$\mathbf{2.856463 \times 10^{-06}}$	4.781680×10^{-05}	2.421558×10^{-05}	$\mathbf{1.214353 \times 10^{-06}}$
0.2	$\mathbf{8.805666 \times 10^{-07}}$	3.535741×10^{-05}	1.233261×10^{-06}	8.706504×10^{-06}	3.312607×10^{-05}	$\mathbf{3.532873 \times 10^{-08}}$
0.3	5.146110×10^{-06}	2.495271×10^{-05}	$\mathbf{8.119822 \times 10^{-07}}$	1.454172×10^{-05}	1.755399×10^{-05}	$\mathbf{4.475227 \times 10^{-07}}$
0.4	2.780715×10^{-06}	2.560681×10^{-05}	$\mathbf{7.753534 \times 10^{-07}}$	4.615430×10^{-06}	1.804920×10^{-05}	$\mathbf{2.842042 \times 10^{-07}}$
0.5	1.359414×10^{-06}	2.127227×10^{-05}	$\mathbf{5.663649 \times 10^{-07}}$	4.426592×10^{-06}	1.888973×10^{-05}	$\mathbf{2.552623 \times 10^{-07}}$
0.6	9.394572×10^{-07}	1.570394×10^{-05}	$\mathbf{5.437249 \times 10^{-07}}$	9.599460×10^{-06}	1.659002×10^{-05}	$\mathbf{1.624006 \times 10^{-07}}$
0.7	4.026649×10^{-07}	9.583692×10^{-06}	$\mathbf{3.555038 \times 10^{-08}}$	8.586999×10^{-06}	1.037132×10^{-05}	$\mathbf{1.193209 \times 10^{-07}}$
0.8	9.554468×10^{-07}	1.991985×10^{-05}	$\mathbf{1.297162 \times 10^{-08}}$	1.651644×10^{-05}	1.402911×10^{-05}	$\mathbf{3.752629 \times 10^{-07}}$
0.9	6.361145×10^{-07}	5.625482×10^{-05}	$\mathbf{1.278474 \times 10^{-07}}$	4.498823×10^{-05}	7.522469×10^{-05}	$\mathbf{9.783728 \times 10^{-07}}$
1.0	1.073576×10^{-03}	1.483420×10^{-03}	$\mathbf{3.995772 \times 10^{-04}}$	9.093789×10^{-04}	1.069798×10^{-03}	$\mathbf{2.023171 \times 10^{-04}}$

Table 4. Comparison of the absolute errors in solutions for the concentration of PGE obtained by the NARX-LM algorithm with different machine learning techniques for Case III and IV.

	Case III			Case IV		
x	FF-NN	LR-NN	NARX-LM	FF-NN	LR-NN	NARX-LM
0.0	5.662392×10^{-05}	1.282375×10^{-04}	$\mathbf{2.454875 \times 10^{-06}}$	9.311650×10^{-05}	2.660996×10^{-04}	$\mathbf{8.705075 \times 10^{-07}}$
0.1	7.540143×10^{-06}	3.653438×10^{-05}	$\mathbf{1.241626 \times 10^{-07}}$	5.827090×10^{-05}	9.107916×10^{-05}	$\mathbf{8.132946 \times 10^{-08}}$
0.2	2.002106×10^{-05}	2.879628×10^{-05}	$\mathbf{5.167114 \times 10^{-09}}$	3.032041×10^{-05}	1.850514×10^{-04}	$\mathbf{6.939629 \times 10^{-09}}$
0.3	3.071841×10^{-05}	4.926253×10^{-05}	$\mathbf{9.863673 \times 10^{-08}}$	5.746880×10^{-05}	3.007176×10^{-05}	$\mathbf{5.252565 \times 10^{-08}}$
0.4	1.557625×10^{-05}	5.678588×10^{-05}	$\mathbf{6.458083 \times 10^{-08}}$	4.507465×10^{-05}	1.119539×10^{-04}	$\mathbf{5.121962 \times 10^{-08}}$
0.5	2.451808×10^{-05}	4.759676×10^{-05}	$\mathbf{7.378733 \times 10^{-08}}$	1.396936×10^{-05}	6.004553×10^{-05}	$\mathbf{4.057286 \times 10^{-08}}$
0.6	7.209635×10^{-06}	2.690070×10^{-05}	$\mathbf{6.402087 \times 10^{-08}}$	5.687769×10^{-05}	1.139300×10^{-04}	$\mathbf{7.379871 \times 10^{-08}}$
0.7	2.222096×10^{-05}	1.090769×10^{-04}	$\mathbf{4.285971 \times 10^{-08}}$	5.169435×10^{-05}	1.277712×10^{-04}	$\mathbf{2.756274 \times 10^{-08}}$
0.8	1.854701×10^{-05}	2.853953×10^{-05}	$\mathbf{1.863085 \times 10^{-07}}$	7.419310×10^{-07}	3.113386×10^{-05}	$\mathbf{5.949529 \times 10^{-09}}$
0.9	$\mathbf{4.618550 \times 10^{-09}}$	1.901168×10^{-04}	5.167832×10^{-07}	3.146698×10^{-05}	1.796623×10^{-04}	$\mathbf{3.940062 \times 10^{-08}}$
1.0	1.150652×10^{-03}	1.836329×10^{-03}	$\mathbf{7.934356 \times 10^{-05}}$	1.193031×10^{-03}	2.681365×10^{-03}	$\mathbf{2.036388 \times 10^{-04}}$

6. Conclusions

In this paper, we examined the system of nonlinear differential equations that relates the steady state concentration of carbon dioxide and phenyl glycidyl ether. To study the chemical analysis and absorption of carbon dioxide (CO_2) into phenyl glycidyl ether (PGE) solutions, a novel stochastic technique based on nonlinear autoregressive exogenous (NARX) neural networks with the Levenberg–Marquardt algorithm was designed. The design scheme NARX-LM algorithm with two different activations function (Log-sigmoid and Hyperbolic tangent) was implemented to investigate the influence of variations in normalized parameters, , such as $\alpha_1, \alpha_2, \beta_1$, and β_2 on concentration profiles of CO_2 and PGE.

Extensive graphical and statistical analysis illustrated that increases in k increased the concentration of CO_2. The diffusivity of PGE decreased with increases in β_1 and β_2. The approximate solutions obtained by the NARX-LM algorithm were compared with state-of-the-art techniques. Statistics dictates that the designs scheme overlapped the numerical solutions with minimum absolute errors. Convergence graphs and error histograms analysis further validated the worth of the design scheme.

References

1. Choe, Y.S.; Park, S.W.; Park, D.W.; Oh, K.J.; Kim, S.S. Reaction kinetics of carbon dioxide with phenyl glycidyl ether by TEA-CP-MS41 catalyst. *J. Jpn. Pet. Inst.* **2010**, *53*, 160–166. [CrossRef]
2. Park, S.W.; Park, D.W.; Kim, T.Y.; Park, M.Y.; Oh, K.J. Chemical kinetics of the reaction between carbon dioxide and phenyl glycidyl ether using Aliquat 336 as a catalyst. *Catal. Today* **2004**, *98*, 493–498. [CrossRef]
3. Inoue, S.; Yamazaki, N. *Organic and Bio-Organic Chemistry of Carbon Dioxide*; Halsted Press: Ultimo, Australia, 1982.
4. Han, L.; Choi, H.J.; Kim, D.K.; Park, S.W.; Liu, B.; Park, D.W. Porous polymer bead-supported ionic liquids for the synthesis of cyclic carbonate from CO_2 and epoxide. *J. Mol. Catal. A Chem.* **2011**, *338*, 58–64. [CrossRef]
5. Sun, J.; Wang, J.; Cheng, W.; Zhang, J.; Li, X.; Zhang, S.; She, Y. Chitosan functionalized ionic liquid as a recyclable biopolymer-supported catalyst for cycloaddition of CO_2. *Green Chem.* **2012**, *14*, 654–660. [CrossRef]
6. Srivastava, R.; Srinivas, D.; Ratnasamy, P. Zeolite-based organic–inorganic hybrid catalysts for phosgene-free and solvent-free synthesis of cyclic carbonates and carbamates at mild conditions utilizing CO_2. *Appl. Catal. A Gen.* **2005**, *289*, 128–134. [CrossRef]
7. Aresta, M.; Dibenedetto, A.; Angelini, A. Catalysis for the valorization of exhaust carbon: From CO_2 to chemicals, materials, and fuels. Technological use of CO_2. *Chem. Rev.* **2014**, *114*, 1709–1742. [CrossRef]
8. Choe, Y.S.; Oh, K.J.; Kim, M.C.; Park, S.W. Chemical absorption of carbon dioxide into phenyl glycidyl ether solution containing THA-CP-MS41 catalyst. *Korean J. Chem. Eng.* **2010**, *27*, 1868–1875. [CrossRef]
9. Singha, R.; Wazwaz, A.M. Steady-state concentrations of carbon dioxide absorbed into phenyl glycidyl ether: An optimal homotopy analysis method. *Match-Commun Math. Co* **2019**, *81*, 800–812.
10. Subramaniam, M.; Krishnaperumal, I.; Lakshmanan, R. Theoretical analysis of mass transfer with chemical reaction using absorption of carbon dioxide into phenyl glycidyl ether solution. *Appl. Math.* **2012**, *3*, 1179–1186. [CrossRef]
11. Morales-Delgado, V.F.; Gómez-Aguilar, J.F.; Yépez-Martínez, H.; Baleanu, D.; Escobar-Jimenez, R.F.; Olivares-Peregrino, V.H. Laplace homotopy analysis method for solving linear partial differential equations using a fractional derivative with and without kernel singular. *Adv. Differ. Equations* **2016**, *2016*, 1–17. [CrossRef]

12. Gómez-Aguilar, J.; Yépez-Martínez, H.; Torres-Jiménez, J.; Córdova-Fraga, T.; Escobar-Jiménez, R.; Olivares-Peregrino, V. Homotopy perturbation transform method for nonlinear differential equations involving to fractional operator with exponential kernel. *Adv. Differ. Equations* **2017**, *2017*, 1–18. [CrossRef]

13. Singh, R. Optimal homotopy analysis method for the non-isothermal reaction–diffusion model equations in a spherical catalyst. *J. Math. Chem.* **2018**, *56*, 2579–2590. [CrossRef]

14. Acan, O.; Baleanu, D. A new numerical technique for solving fractional partial differential equations. *arXiv* **2017**, arXiv:1704.02575.

15. Kumar, R.; Kumar, S.; Singh, J.; Al-Zhour, Z. A comparative study for fractional chemical kinetics and carbon dioxide CO_2 absorbed into phenyl glycidyl ether problems. *AIMS Math* **2020**, *5*, 3201–3222. [CrossRef]

16. Sulaiman, M.; Samiullah, I.; Hamdi, A.; Hussain, Z. An improved whale optimization algorithm for solving multi-objective design optimization problem of PFHE. *J. Intell. Fuzzy Syst.* **2019**, *37*, 3815–3828. [CrossRef]

17. Wu, X.; Shen, J.; Li, Y.; Lee, K.Y. Data-driven modeling and predictive control for boiler–turbine unit using fuzzy clustering and subspace methods. *ISA Trans.* **2014**, *53*, 699–708. [CrossRef] [PubMed]

18. Ahmad, S.; Sulaiman, M.; Kumam, P.; Hussain, Z.; Asif Jan, M.; Mashwani, W.K.; Ullah, M. A novel population initialization strategy for accelerating levy flights based multi-verse optimizer. *J. Intell. Fuzzy Syst.* **2020**, *39*, 1–17. [CrossRef]

19. Khan, N.A.; Sulaiman, M.; Aljohani, A.J.; Kumam, P.; Alrabaiah, H. Analysis of multi-phase flow through porous media for imbibition phenomena by using the LeNN-WOA-NM algorithm. *IEEE Access* **2020**, *8*, 196425–196458. [CrossRef]

20. Wu, X.; Shen, J.; Wang, M.; Lee, K.Y. Intelligent predictive control of large-scale solvent-based CO_2 capture plant using artificial neural network and particle swarm optimization. *Energy* **2020**, *196*, 117070. [CrossRef]

21. Xi, H.; Wu, X.; Chen, X.; Sha, P. Artificial intelligent based energy scheduling of steel mill gas utilization system towards carbon neutrality. *Appl. Energy* **2021**, *295*, 117069. [CrossRef]

22. Chen, X.; Wu, X.; Lee, K.Y. The mutual benefits of renewables and carbon capture: Achieved by an artificial intelligent scheduling strategy. *Energy Convers. Manag.* **2021**, *233*, 113856. [CrossRef]

23. Khan, N.A.; Sulaiman, M.; Kumam, P.; Aljohani, A.J. A new soft computing approach for studying the wire coating dynamics with Oldroyd 8-constant fluid. *Phys. Fluids* **2021**, *33*, 036117. [CrossRef]

24. Waseem, W.; Sulaiman, M.; Alhindi, A.; Alhakami, H. A soft computing approach based on fractional order DPSO algorithm designed to solve the corneal model for eye surgery. *IEEE Access* **2020**, *8*, 61576–61592. [CrossRef]

25. Khan, A.; Sulaiman, M.; Alhakami, H.; Alhindi, A. Analysis of oscillatory behavior of heart by using a novel neuroevolutionary approach. *IEEE Access* **2020**, *8*, 86674–86695. [CrossRef]

26. Huang, W.; Jiang, T.; Zhang, X.; Khan, N.A.; Sulaiman, M. Analysis of beam-column designs by varying axial load with internal forces and bending rigidity using a new soft computing technique. *Complexity* **2021**, *2021*, 6639032. [CrossRef]

27. Zhang, Y.; Lin, J.; Hu, Z.; Khan, N.A.; Sulaiman, M. Analysis of Third-Order Nonlinear Multi-Singular Emden–Fowler Equation by Using the LeNN-WOA-NM Algorithm. *IEEE Access* **2021**, *9*, 72111–72138. [CrossRef]

28. Wu, X.; Wang, M.; Shen, J.; Li, Y.; Lawal, A.; Lee, K.Y. Reinforced coordinated control of coal-fired power plant retrofitted with solvent based CO_2 capture using model predictive controls. *Appl. Energy* **2019**, *238*, 495–515. [CrossRef]

29. Khan, N.A.; Khalaf, O.I.; Romero, C.A.T.; Sulaiman, M.; Bakar, M.A. Application of Euler Neural Networks with Soft Computing Paradigm to Solve Nonlinear Problems Arising in Heat Transfer. *Entropy* **2021**, *23*, 1053. [CrossRef]

30. Waseem, W.; Sulaiman, M.; Kumam, P.; Shoaib, M.; Raja, M.A.Z.; Islam, S. Investigation of singular ordinary differential equations by a neuroevolutionary approach. *PLoS ONE* **2020**, *15*, e0235829. [CrossRef]

31. Ahmad, A.; Sulaiman, M.; Alhindi, A.; Aljohani, A.J. Analysis of temperature profiles in longitudinal fin designs by a novel neuroevolutionary approach. *IEEE Access* **2020**, *8*, 113285–113308. [CrossRef]

32. Araújo, R.d.A.; Oliveira, A.L.; Meira, S. A morphological neural network for binary classification problems. *Eng. Appl. Artif. Intell.* **2017**, *65*, 12–28. [CrossRef]

33. Gong, T.; Fan, T.; Guo, J.; Cai, Z. GPU-based parallel optimization of immune convolutional neural network and embedded system. *Eng. Appl. Artif. Intell.* **2017**, *62*, 384–395. [CrossRef]

34. Yu, S.; Zhu, K.; Zhang, X. Energy demand projection of China using a path-coefficient analysis and PSO–GA approach. *Energy Convers. Manag.* **2012**, *53*, 142–153. [CrossRef]

35. Rabin, R.; Stewart, V. Dual response regulators (NarL and NarP) interact with dual sensors (NarX and NarQ) to control nitrate-and nitrite-regulated gene expression in Escherichia coli K-12. *J. Bacteriol.* **1993**, *175*, 3259–3268. [CrossRef] [PubMed]

36. Ardalani-Farsa, M.; Zolfaghari, S. Chaotic time series prediction with residual analysis method using hybrid Elman–NARX neural networks. *Neurocomputing* **2010**, *73*, 2540–2553. [CrossRef]

37. Boussaada, Z.; Curea, O.; Remaci, A.; Camblong, H.; Mrabet Bellaaj, N. A nonlinear autoregressive exogenous (NARX) neural network model for the prediction of the daily direct solar radiation. *Energies* **2018**, *11*, 620. [CrossRef]

38. Menezes, J.M.P., Jr.; Barreto, G.A. Long-term time series prediction with the NARX network: An empirical evaluation. *Neurocomputing* **2008**, *71*, 3335–3343. [CrossRef]

39. Kodogiannis, V.; Lisboa, P.J.; Lucas, J. Neural network modelling and control for underwater vehicles. *Artif. Intell. Eng.* **1996**, *10*, 203–212. [CrossRef]

40. De Giorgi, M.G.; Ficarella, A.; Quarta, M. Dynamic performance simulation and control of an aeroengine by using NARX models. In *MATEC Web of Conferences*; EDP Sciences: Les Ulis, France, 2019; Volume 304, p. 03005.

41. Duan, J.S.; Rach, R.; Wazwaz, A.M. Steady-state concentrations of carbon dioxide absorbed into phenyl glycidyl ether solutions by the Adomian decomposition method. *J. Math. Chem.* **2015**, *53*, 1054–1067. [CrossRef]
42. Al-Jawary, M.; Raham, R.; Radhi, G. An iterative method for calculating carbon dioxide absorbed into phenyl glycidyl ether. *J. Math. Comput. Sci.* **2016**, *6*, 620–632.
43. Saranya, K.; Mohan, V.; Rajendran, L. Steady-state concentrations of carbon dioxide absorbed into phenyl glycidyl ether solutions by residual method. *J. Math. Chem.* **2020**, *58*, 1230–1246. [CrossRef]